Ecosystem Health and Sustainability
A SCIENCE PARTNER JOURNAL

RESEARCH ARTICLE

Resistance and Resilience of Vegetation and Microclimate along the Subtropical Expressway via Remote Sensing

Jiali Gu[1†], Wan Geng[1†], Zhouyuan Li[1,2,*], Brian D. Fath[3,4], Fei Pan[1], Haiyue Shi[1], Jiding Chen[5], Yaping Kong[5], Shuangcheng Tao[5], and Guilong Song[1,6*]

[1]School of Grassland Science, Beijing Forestry University, Beijing 100083, China. [2]Key Laboratory for Earth Surface Processes of the Ministry of Education, Peking University, Beijing 100871, China. [3]Department of Biological Sciences, Towson University, Towson, MD 21252-0001, USA. [4]Advancing Systems Analysis Program, International Institute for Applied Systems Analysis, Laxenburg 2361, Austria. [5]Center for Environmental Protection and Soil and Water Conservation, China Academy of Transportation Sciences, Beijing 100013, China. [6]Engineering and Technology Research Center for Sports Field and Slope Protection Turf, National Forestry and Grassland Administration, Beijing 100083, China.

*Address correspondence to: lizhouyuan@bjfu.edu.cn (Z.L.); syihan@163.com (G.S.)
†These authors contributed equally to this work.

Citation: Gu J, Geng W, Li Z, Fath BD, Pan F, Shi H, Chen J, Kong Y, Tao S, Song G. Resistance and Resilience of Vegetation and Microclimate along the Subtropical Expressway via Remote Sensing. *Ecosyst. Health Sustain.* 2026;12:Article 0509. https://doi.org/10.34133/ehs.0509

Submitted 2 September 2025
Revised 17 January 2026
Accepted 4 March 2026
Published 8 April 2026

Evaluating vegetation resistance and resilience is key to understanding ecosystem responses to human disturbances such as road construction and to guiding ecological restoration. This study systematically assessed the resistance and resilience of vegetation and microclimate along the Hangrui Expressway in southwestern China using remote sensing techniques. Landsat imagery from 10 representative years between the preconstruction period (1993) and the recovery period (2021) was analyzed, with indicators such as the normalized difference vegetation index, surface temperature, and evapotranspiration used to characterize vegetation and microclimate. The study area was divided into 200-m buffer zones, and resistance–resilience indicators were developed to reveal spatial distribution patterns. In addition, an optimized "forest–grassland ratio" was proposed to guide vegetation configuration strategies, effectively promoting the enhancement of both vegetation and microclimate resilience. Structural equation modeling identified the key factors influencing roadside vegetation resistance and resilience. The results showed that most areas exhibited strong resistance and resilience, enabling rapid recovery after disturbances. Vegetation typically required about 4 years to recover, while surface temperature and evapotranspiration required 7 and 2 years, respectively, to return to predisturbance levels. Topographic factors were significantly positively correlated with microclimate resilience, while climate factors were positively correlated with microclimate resilience but negatively correlated with vegetation resilience. Climate and topography were the main influencing factors. The optimal forest–grassland ratio varied across different regions. These findings underscore the importance of considering local climatic and topographic conditions in road planning and ecological restoration to improve restoration outcomes and promote ecosystem stability.

Introduction

With the increasing frequency of anthropogenic disturbances and climate change, evaluating the ability of ecosystems to maintain stability and function before and after disturbance events has become a central issue in ecological research. Resistance and resilience are 2 critical indicators widely used in the assessment of ecosystem stability and sustainability, as well as in ecological restoration practices. The concept of resilience was first proposed by Holling [1], defining it as the capacity of an ecosystem to absorb disturbances and return to its original state. Gauch et al. [2] expanded this concept by highlighting that resilience is not only temporal but also involves spatial patterns, structural integrity, functional performance, and system adaptability. Pimm [3] further emphasized that resilience manifests differently at various ecological scales, such as species, community, and ecosystem levels. The Intergovernmental Panel on Climate Change [4] extended the definition of climate system resilience to include the capacity to sustain core functions while adapting to and transforming under environmental change. In contrast, resistance refers to the system's ability to maintain its structure and function during disturbances [5]. In ecological studies, resistance

is often measured by the intensity of vegetation response under climatic anomalies [6,7]. Holling's adaptive cycle model, "Panarchy", provides a theoretical framework for understanding ecosystem dynamics, dividing ecosystem development into 4 stages: exploitation (r), conservation (K), release (Ω), and reorganization (α). Resistance tends to dominate during the K phase, while resilience becomes critical in the Ω and α phases. This model promotes a paradigm shift from static recovery to adaptive restoration in ecological management [8]. His study defines resistance as the ability of an ecosystem to maintain or return to its predisturbance level after experiencing a disturbance, while resilience refers to the time required for an ecosystem to recover to its predisturbance state.

In practical applications, resistance and resilience are extensively used to guide restoration strategies across different ecosystem types. For instance, in forest and wetland restoration, assessing ecosystem resilience is essential for determining the appropriate intensity and type of intervention [9,10]. Studies have shown that natural geographic factors, such as elevation and slope, positively influence resilience, whereas climatic extremes—such as excessive rainfall or temperature fluctuations—may negatively affect the recovery process [11]. In addition, differences in restoration measures and human activities lead to spatial heterogeneity in resilience and resistance across landscapes [12–15].

In recent years, the rapid expansion of China's expressway network has imposed substantial ecological pressure on surrounding environments. Road construction not only alters local microclimate conditions, soil structures, and biological habitats but also creates urgent demands for ecological restoration and reconstruction [16]. Artificial vegetation restoration has proven effective in enhancing regional ecological functions by improving soil retention, regulating water cycles, and maintaining biodiversity. Moreover, it contributes to the improvement of highway environmental quality and supports regional sustainable development [17].

As a crucial component of ecological engineering, expressway greening, through the rational configuration of trees, shrubs, and herbaceous vegetation, plays an important role in mitigating construction-induced disturbances and enhancing ecosystem structural stability and service functions [18–20]. However, although the ecological effects of highway construction have been widely investigated, the structural regulatory role of the forest–grassland ratio (FGR) in ecological restoration has not yet been systematically examined. As ecological restoration progresses, vegetation communities gradually establish relatively stable configuration patterns. The FGR represents the structural optimization of plant communities during their adaptation to environmental conditions and is strongly associated with vegetation resistance, microclimate regulation, and ecosystem service functions. Studies have demonstrated that optimizing FGR can help regulate land surface temperature and improve the responsiveness and recovery efficiency of vegetation systems under disturbance [21,22].

The advancement of remote sensing technology has provided strong support for large-scale, long-term monitoring and assessment of ecosystems. Remote sensing enables continuous observation of key ecological variables such as the normalized difference vegetation index (*NDVI*), land surface temperature (*Ts*), and evapotranspiration (*ET*), significantly improving the spatial quantification of ecosystem resistance and resilience [23]. *NDVI* reflects vegetation cover and growth status and is positively correlated with vegetation density [24]. *Ts* indicates the regional thermal environment and the vegetation–microclimate interaction, retrievable via thermal infrared bands [25]. *ET*, a key process in energy and water cycles, can be efficiently estimated at the pixel level using energy balance models and remote sensing data [26]. In the context of transportation infrastructure, remote sensing effectively reveals the ecological impacts of road construction, offering scientific support for restoration planning in disturbed areas [27].

Despite marked progress in assessing ecosystem resistance and resilience, quantitative investigations into the long-term ecological disturbances caused by road construction and the subsequent recovery processes remain limited. To fill this gap, this study takes the Hangrui Expressway in Yunnan Province as a case study and utilizes multitemporal remote sensing data from 1993 to 2021. The objectives are to (a) clarify whether topographic and microclimatic factors (e.g., elevation, slope, temperature, and precipitation) significantly affect the resistance and resilience of roadside vegetation along the expressway and (b) evaluate whether optimizing the FGR can effectively enhance the ecological resistance and resilience of expressway ecosystems. This study aims to systematically assess the ecological disturbances induced by expressway construction and their subsequent recovery processes, thereby providing theoretical insights and scientific support for ecological restoration and sustainable infrastructure development in transportation-impacted landscapes.

Materials and Methods

Study area

The study area is selected along the Hangrui Expressway in Yunnan, covering 6 sections from east to west, as shown in Table 1: Qujing–Songming section, Kunming–Songming section, Kunming Second Ring Road, Anning–Chuxiong section, Chuxiong–Dali section, and Dali–Baoshan section, with a total length of approximately 1,036.3 km, as shown in Fig. 1. The Hangrui Expressway, officially known as the Hangzhou–Ruili Expressway, is an expressway connecting Hangzhou in Zhejiang Province to Ruili in Yunnan Province.

Yunnan Province has a diverse range of climate types, primarily characterized by a subtropical plateau monsoon climate with distinct wet and dry seasons. In 2023, the annual average precipitation was 887.1 mm. The rainy season lasts from May to October, and the dry season extends from November to April. Temperature variations with altitude are exceptionally pronounced.

Table 1. Information on different sections in the study area

Section name	Expressway opening date (year)	Total length (km)
Qujing–Songming	2007	136.18
Kunming–Songming	1996	130.69
Kunming Second Ring Road	1995	–
Anning–Chuxiong	2005	129.93
Chuxiong–Dali	1998	178.78
Dali–Baoshan	2002	165.64

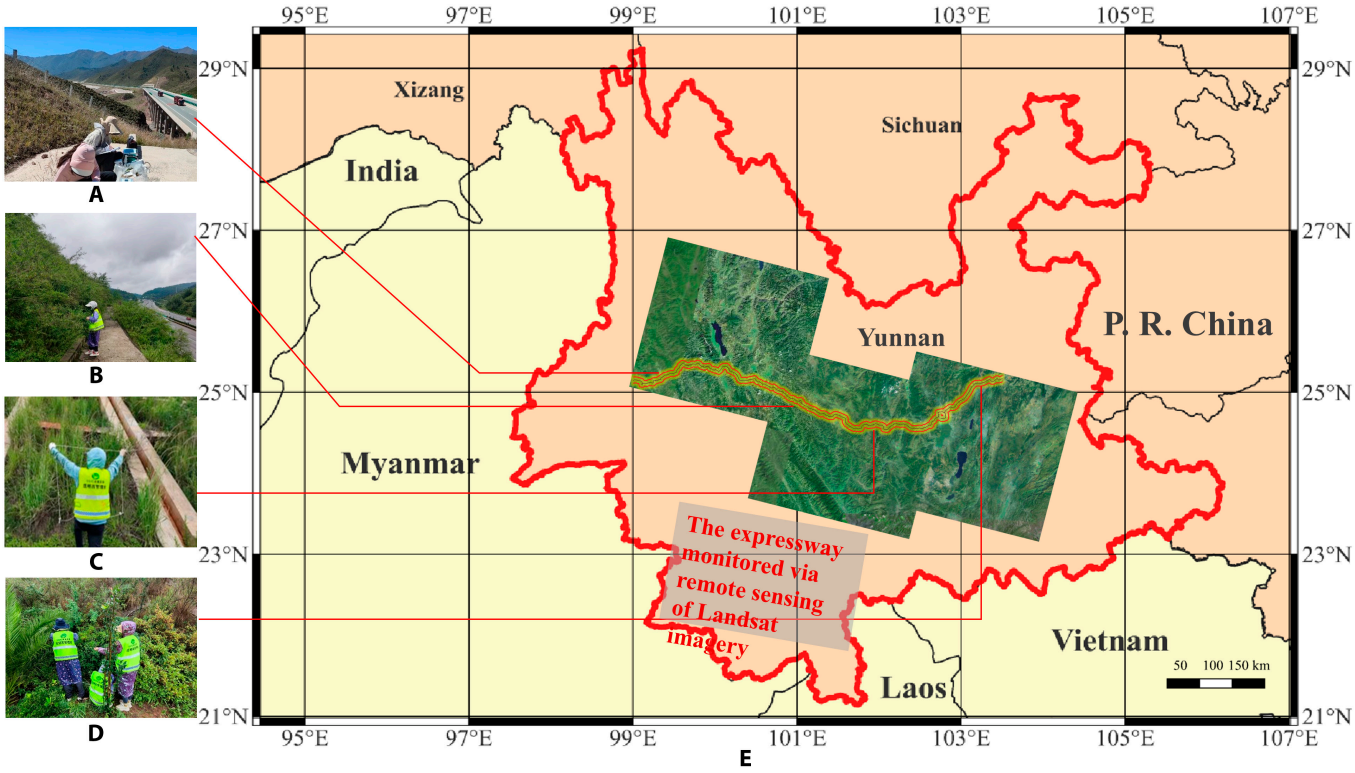

Fig. 1. (A to D) Field survey photographs of ecological restoration at different locations along the Hangrui Expressway in Yunnan. (E) The map and satellite imagery of the study area along the Hangrui Expressway in Yunnan.

Data collection

The remote sensing data used in the study were sourced from Landsat 4-5 Thematic Mapper (TM) and Landsat 8 Operational Land Imager (OLI) / Thermal Infrared Sensor (TIRS). Ten years were selected from the 28-year recovery period between 1993 and 2021, namely, 1993 (1994), 1996, 2003 (2004), 2007, 2009, 2011 (2013), 2014, 2017, 2019, and 2021, representing different recovery stages of the Yunnan section of the Hangrui Expressway. Through the Geospatial Data Cloud website (www.gscloud.cn), 30 remote sensing images with a range of 30 × 30 km and a spatial resolution of 30 m were downloaded. The selected data were from the vegetation growing season (March to May), with cloud cover less than 10%. Detailed information about the data can be found in Table 2. In addition, the 30-m land cover dataset and its dynamics for China from 1990 to 2019 were used as the basis for Land-Use and Land-Cover Change (LUCC) classification [28]. The digital elevation model (DEM) data used in this study are sourced from the Geospatial Data Cloud website (http://www.gscloud.cn/), specifically the GDEMV3 (Global Digital Elevation Model Version 3) data with a spatial resolution of 30 m. Slope calculations were performed in QGIS. The annual average temperature and annual precipitation data (26 periods from 1990 to 2015) are derived from the national meteorological interpolation data products provided by the Resource and Environmental Science and Data Center of the Chinese Academy of Sciences, with a spatial resolution of 1 km.

The remote sensing data used in this study are sourced from publicly available platforms, freely available for academic research without special licensing. The data copyright is held by NASA and the US Geological Survey. We comply with the relevant copyright and ethical standards.

Satellite imagery data preprocessing

Based on the vector map of the Hangrui Expressway in Yunnan, a 200-m buffer zone was delineated along both sides of the expressway. The 200-m buffer was selected through preliminary testing, balancing roadside vegetation characteristics, data coverage, and long-term monitoring requirements, and is suitable for capturing landscape-scale vegetation recovery and microclimatic effects. Using the "Vector-Geoprocessing Tools-Create Grid" function in QGIS, the 150-km^2 area was divided into 30,415 grids, each measuring 90 × 90 m, for spatial statistical analysis. Subsequently, the *NDVI*, *Ts*, and *ET* indicator images were clipped using the buffer zone as the vector shape, facilitating the extraction and comparison of data for further analysis.

Using QGIS, the study area's land use/land cover changes from 1993 to 2019 were clipped, mapped, and sampled. Based on the defined buffer zone, a central point was created for each pixel, and sampling was conducted by matching points to raster images to obtain a dataset. The values for each pixel were extracted, including annual LUCC information for each grid point (covering trees, shrubs, and grasslands). Finally, the pixel values of the raster dataset were extracted and analyzed. A schematic diagram of the buffer zone and grid division is shown in Fig. 2.

Resistance–resilience assessment

A resistance–resilience index is constructed using long-term time series remote sensing data, with *NDVI*, *Ts,* and *ET* serving as indicators representing artificial vegetation and surface microclimate factors, respectively. This index decomposes the fluctuation process of damaged ecosystem states, identifies inflection points in dynamic succession, and quantifies the

Table 2. List of Landsat remote sensing data selected for the study

Study area (path/row)	Satellite sensor	Acquisition date (yyyy-mm-dd)
Dali–Baoshan, Chuxiong–Dali sections (131/42)	Landsat 5 TM	1993(1994)-03-10
	Landsat 5 TM	1996-03-02
	Landsat 5 TM	2003(2004)-03-22
	Landsat 5 TM	2007-03-01
	Landsat 5 TM	2009-03-22
	Landsat 5 TM	2011(2013)-04-13
	Landsat 8 OLI/TIRS	2014-04-21
	Landsat 8 OLI/TIRS	2017-03-28
	Landsat 8 OLI/TIRS	2019-03-18
	Landsat 8 OLI/TIRS	2021-03-23
Anning–Chuxiong, Kunming Second Ring Road sections (130/43)	Landsat 4 TM	1993(1994)-03-11
	Landsat 5 TM	1996-04-12
	Landsat 5 TM	2004-03-17
	Landsat 5 TM	2007-03-10
	Landsat 5 TM	2009-04-16
	Landsat 5 TM	2011(2013)-04-06
	Landsat 8 OLI/TIRS	2014-04-14
	Landsat 8 OLI/TIRS	2017-04-06
	Landsat 8 OLI/TIRS	2019-05-14
	Landsat 8 OLI/TIRS	2021-03-16
Kunming–Songming, Qujing–Songming sections (129/43)	Landsat 5 TM	1994-03-15
	Landsat 5 TM	1996-04-05
	Landsat 5 TM	2003(2004)-04-09
	Landsat 5 TM	2007-05-06
	Landsat 5 TM	2009-03-24
	Landsat 8 OLI/TIRS	2013-04-20
	Landsat 8 OLI/TIRS	2014-03-06
	Landsat 8 OLI/TIRS	2017-05-01
	Landsat 8 OLI/TIRS	2019-05-07
	Landsat 8 OLI/TIRS	2021-03-25

periodic rebound cycles. The upper quartile values of *NDVI*, *Ts*, and *ET* (representing predisturbance vegetation greenness and surface microclimate factor levels) are used as criteria for equilibrium states. A sliding difference method is used to determine the apex of each fluctuation cycle, constructing "degradation-bottom-recovery" triangles (as shown in Fig. 3). During the construction of expressways, vegetation is damaged to a trough, and after the first phase of artificial vegetation restoration, it reaches equilibrium again. However, it continues to be subjected to disturbances, causing it to deviate from equilibrium. Through resistance and recovery processes, artificial vegetation gradually returns to equilibrium, experiencing fluctuations over a long time series.

In this model, the distance from the trough to the equilibrium state is defined as resistance (a), while the time taken for the trough to return to equilibrium is defined as resilience (b). Due to ongoing external disturbances during the recovery process of artificial vegetation and surface microclimate factors, multiple fluctuations occur, with each deviation from and return to equilibrium forming a new triangle. These fluctuations are used to measure the recovery process of damaged vegetation and surface microclimate factors. The model allows for the assessment of vegetation resistance (*RS*) and resilience (*RL*) over a specified period, which was calculated using the following formulae:

$$RS = 1 / \left(\sum a_i / n \right) \quad (1)$$

$$RL = 1 / \left(\sum b_i / n \right) \quad (2)$$

where a_i represents the resistance capability of each fluctuation cycle in the vertical direction as the measurement for combating disturbance, b_i represents the resilience capability of each fluctuation cycle in the horizontal direction as the measurement for recovery after disturbance, and n denotes the number of fluctuation cycles.

Calculation on vegetational and microclimate indicators

After data preprocessing, *NDVI* and *Ts* were calculated using the "Raster Calculator" in QGIS, while *ET* was calculated using ERDAS and its modeler functions. The A Spatially-Adaptive Fast Atmospheric Correction-2 (ATCOR 2) module in ERDAS IMAGINE 2011 was used to calculate surface energy balance and heat flux as a value-added product. The ATCOR 2 module serves as an atmospheric correction tool for flat terrains, enabling the calculation of ground reflectance and *Ts* using satellite data.

Normalized difference vegetation index

Healthy green vegetation has strong reflectance in the near-infrared band and strong absorption in the visible light band. The combination of Landsat's red and near-infrared bands is used to calculate the vegetation index, with *NDVI* calculated using QGIS software, where NIR represents the near-infrared band and red represents the red band.

$$NDVI = (\mathrm{NIR} - \mathrm{red}) / (\mathrm{NIR} + \mathrm{red}) \quad (3)$$

Surface temperature

For Landsat thermal infrared data, the surface radiant temperature is estimated on the basis of the principles of Planck's blackbody radiation formula and its variant forms. A specific calculation expression for *Ts* was derived and established for use with Landsat TM/Enhanced TM data [29].

$$Ts = K_2 / \ln\left(K_1 \varepsilon / \rho_{\mathrm{TIR}} + 1\right) \quad (4)$$

where is one of the radiance constants for band 6 of the remote sensing image: $K_1 = 607.76\ \mathrm{W{\cdot}m^{-2}{\cdot}sr^{-1}{\cdot}\mu m^{-1}}$ for Landsat 5 and $K_1 = 774.89\ \mathrm{W{\cdot}m^{-2}{\cdot}sr^{-1}{\cdot}\mu m^{-1}}$ for Landsat 8. K_2 is another radiance constant for band 6: $K_2 = 1{,}260.56\ \mathrm{W{\cdot}m^{-2}{\cdot}sr^{-1}{\cdot}\mu m^{-1}}$ for Landsat 5 and $K_2 = 1{,}321.08\ \mathrm{W{\cdot}m^{-2}{\cdot}sr^{-1}{\cdot}\mu m^{-1}}$ for Landsat 8. These values can be found in the Metadata (MTL) file of the remote sensing images. ρ_{TIR} is the spectral reflectance values in the thermal infrared bands of remote sensing (different satellite models may operate in different bands). ε is the surface

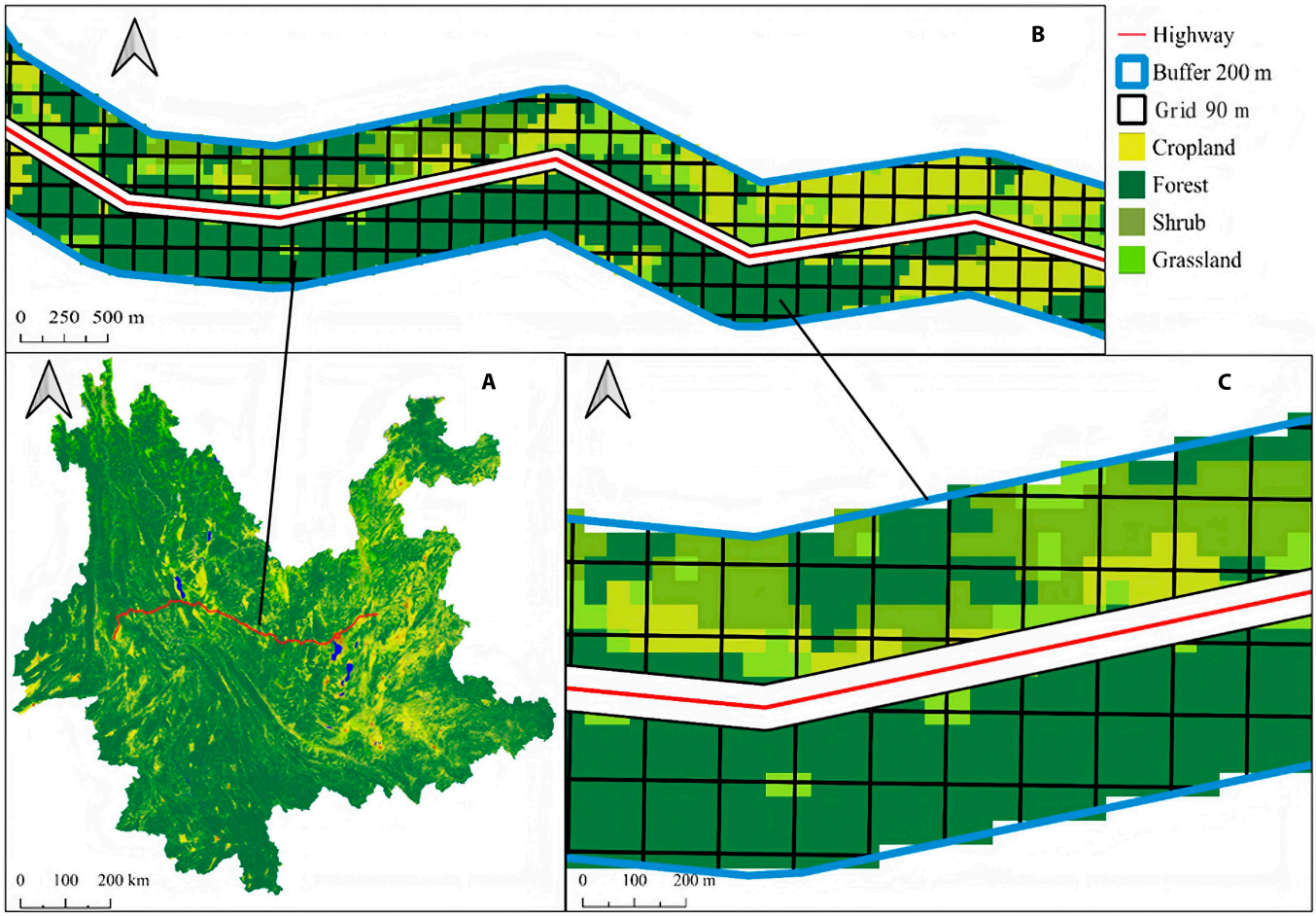

Fig. 2. (A) Schematic diagram of buffer zone grid division. (B) Location map of the Yunnan section of the Hangrui Expressway. (C) Enlarged schematic of the buffer zone grid division, where each grid cell measures 90 × 90 m and contains various vegetation types, including cropland, forest, shrubland, and grassland.

emissivity, calculated using the empirical formula $\varepsilon = 1.009 + 0.047\ln(NDVI)$ when $NDVI > 0$. When $NDVI \leq 0$, the surface is typically considered bare soil or nonvegetated, with minimal influence from vegetation. Therefore, we set ε to 1 in this case. This approach ensures that the calculation process can proceed smoothly even in the absence of effective vegetation, while also avoiding calculation instability caused by negative *NDVI* values.

Evapotranspiration

In this study, the ATCOR 2 computational workstation platform integrated with ERDAS software was used to run the model processing [30,31]. After completing atmospheric correction, the enhanced products were used for modeling calculations. As previously described, the model is based on the surface energy balance model and the conversion of heat flux. Its core foundational formula is the surface energy balance equation.

$$R_n = LE + G + H \tag{5}$$

$$ET = LE / 286 \tag{6}$$

Among them, R_n represents the net radiation flux at the surface ($W{\cdot}m^{-2}$), LE represents the latent heat flux ($W{\cdot}m^{-2}$), G represents the soil heat flux ($W{\cdot}m^{-2}$), and H represents the sensible heat flux ($W{\cdot}m^{-2}$).

The definition of FGR in ecological restoration

The FGR refers to the ratio of the combined area of tree and shrub vegetation to the area of herbaceous vegetation within an artificial vegetation community. This ratio reflects the structure of artificial vegetation along expressways. The concept was introduced to capture the spatial differentiation pattern of artificial vegetation structure. Trees, shrubs, and herbaceous plants each have distinct advantages in terms of ecosystem service functions. Changes in FGR not only influence the resistance–resilience dynamics of vegetation but also impact ecological services such as biodiversity. Therefore, the study of FGR in expressway artificial vegetation is of practical significance for formulating rational vegetation restoration strategies.

The restoration stability index (*ResIndex*) represents the combined performance of resistance and resilience, while Res_{veg_clim} represents the combined performance of vegetation structure and function. Due to the concentrated and skewed distribution of the original data, a logarithmic transformation [as in Eq. (8)] was applied to normalize the data distribution, facilitating subsequent analysis. The optimal FGR is determined by fitting a logarithmic function to the position of Res_{veg_clim}, extracting the inflection point to identify the most suitable FGR.

$$\text{FGR} = (\text{Forest} + \text{Shrub}) / \text{Grassland} \tag{7}$$

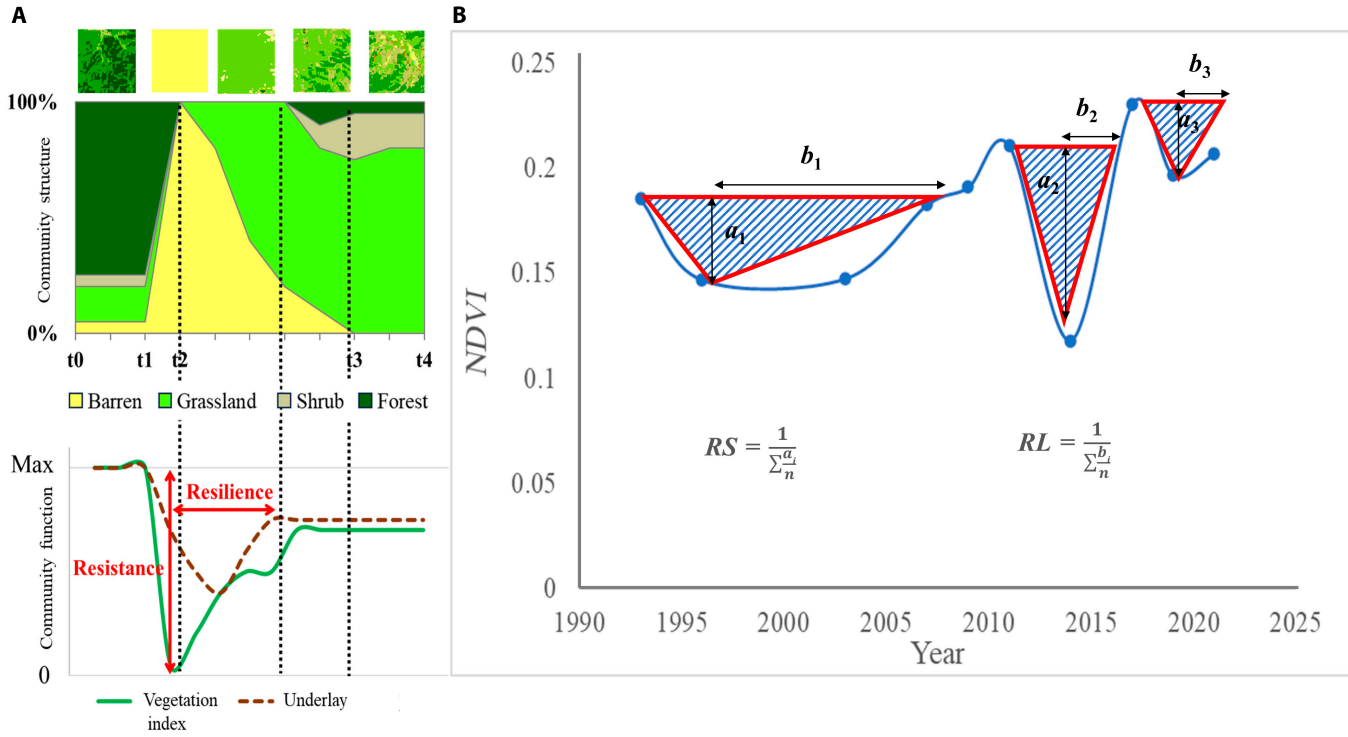

Fig. 3. (A) Conceptual diagram of changes in vegetation community structure and function before and after road construction (t2). (B) Long-term time series resistance–resilience calculation model based on normalized difference vegetation index (*NDVI*) as an indicator.

$$ResIndex = \log(1/(RS+RL)) \quad (8)$$

$$Res_{veg\_clim} = ResIndex_{NDVI} + ResIndex_{Ts} + ResIndex_{ET} \quad (9)$$

Statistical analysis

By statistically analyzing the values of key indicators, vegetation resistance ($NDVI_a$), vegetation resilience ($NDVI_b$), land *Ts* resistance (Ts_a), land *Ts* resilience (Ts_b), *ET* resistance (ET_a), and *ET* resilience (ET_b) frequency distribution maps are created to examine their spatial distribution patterns, revealing the trends in vegetation and microclimate resilience and resistance, providing scientific support for optimizing ecological restoration strategies.

Next, through collecting data on the FGR for different road sections and fitting the relationship between FGR and Res_{veg_clim} using nonlinear functions, the inflection point is determined as the optimal FGR value, quantifying the impact of the FGR on vegetation structure and functional resilience index.

Subsequently, the study examines the impact of natural factors such as average temperature, average precipitation, slope, and altitude on vegetation and microclimate resilience and resistance. The standardized regression coefficients are calculated to assess the impact of these factors on the 6 stability indicators ($NDVI_a$, $NDVI_b$, Ts_a, Ts_b, ET_a, and ET_b). In addition, a structural equation modeling (SEM) is developed and applied to analyze the direct and indirect effects of geographic, climatic, and engineering factors on vegetation and microclimate resilience. It is hypothesized that the vegetation resilience index directly influences the water-heat factor resilience index, and all these indicators are moderated by environmental and engineering factors. In other words, environmental and engineering factors can directly or indirectly influence the resilience index of water-heat factors by affecting the vegetation resilience index. The SEM is fitted using the "piecewiseSEM" package in R, revealing the interactions and influence mechanisms of these factors on resilience and resistance. Effect sizes were quantified using standardized path coefficients, the explained variance (R^2), and Cohen's f^2

$$f^2 = R^2 / (1-R^2) \quad (10)$$

allowing the relative magnitude of each pathway to be interpreted as small (≈0.02), medium (≈0.15), or large (≈0.35) according to conventional criteria [32].

Results

Spatial characteristics of resistance and resilience

The frequency distribution results for vegetation resistance and resilience along the Hangrui Expressway indicate that the vegetation exhibits strong resistance and resilience overall after being disturbed. Spatially, both $NDVI_a$ and $NDVI_b$ show spatial heterogeneity. From the frequency distribution analysis of the entire expressway, the $NDVI_a$ values exhibit a right-skewed distribution, with most samples having low $NDVI_a$ values, indicating strong resistance. The largest proportion of samples falls within the range of 0 to 0.32, accounting for 98.4%, with a mode of 0.16. This indicates that the resistance of 98.4% of the grid cells is concentrated within this range. Only 0.16% of the samples have higher $NDVI_a$ values, suggesting that areas with weak resistance account for just 0.16%.

Similarly, the frequency distribution for $NDVI_b$ also shows a right-skewed pattern, with the highest proportion of samples in the range of 2 to 6.4, accounting for 51.5%, with a mode of

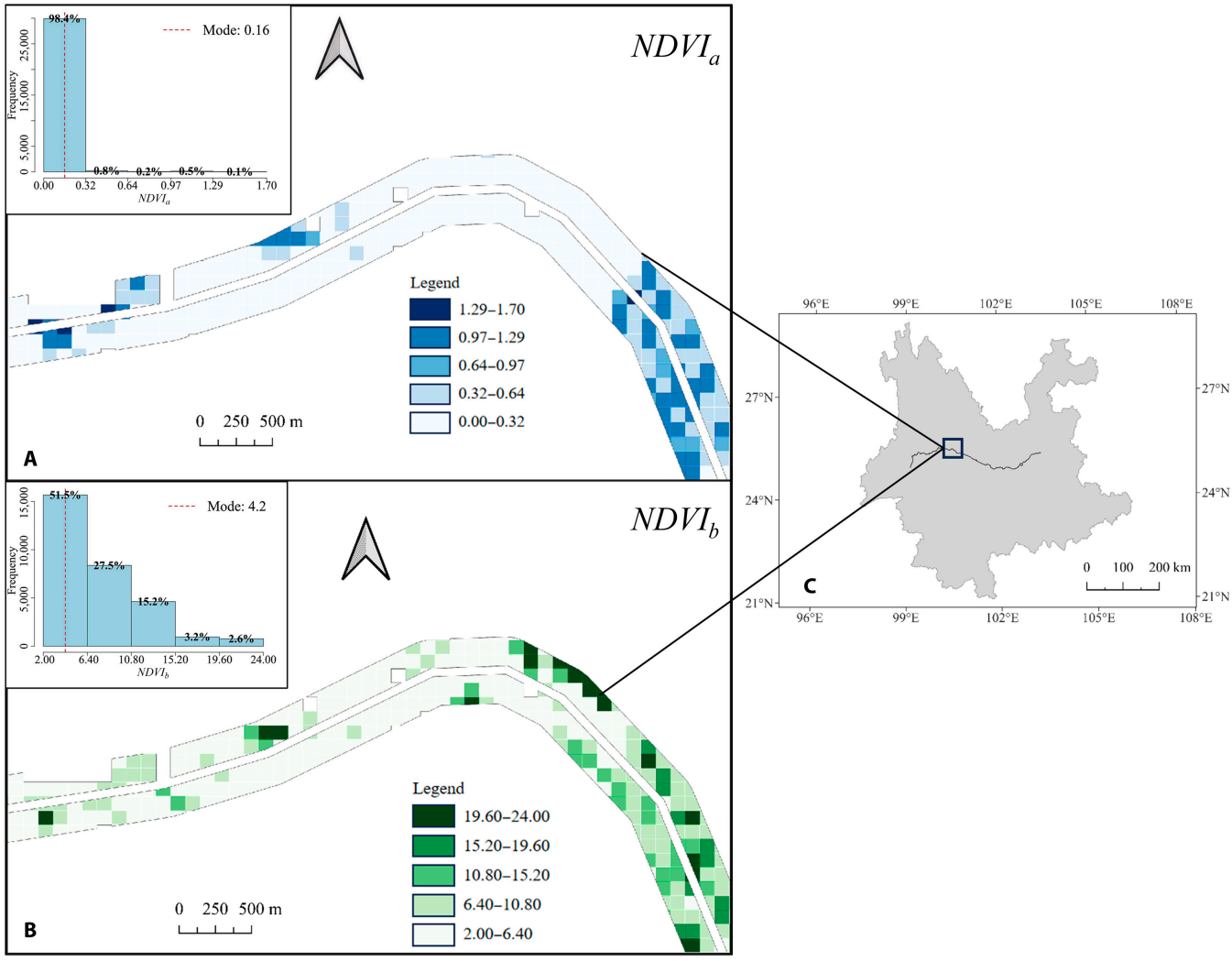

Fig. 4. The spatial distribution is based on locally enlarged sections of the Hangrui Expressway in Yunnan, while the frequency distribution is derived from data collected along the entire expressway. (A) $NDVI_a$ represents vegetation resistance (range, 0 to 1.70), with darker colors indicating weaker resistance. (B) $NDVI_b$ represents vegetation resilience (range, 2 to 24), with darker colors indicating weaker resilience. (C) Locations of the enlarged study sections within Yunnan Province.

4.2. This suggests that most of the areas along the expressway have artificial vegetation that takes about 4 years to recover to predisturbance levels of vegetation greenness.

The spatial and frequency distribution results for the surface water-heat factors' resistance and resilience along the Hangrui Expressway indicate that these factors demonstrate strong overall resistance to disturbances, with *Ts* recovering slowly and *ET* recovering quickly. Spatial analysis of the expressway reveals significant heterogeneity in both Ts_a and Ts_b.

From the frequency distribution analysis of the entire expressway, the Ts_a values exhibit a right-skewed distribution. This indicates that the *Ts* is relatively stable in 95.6% of the grid areas. The largest proportion of samples falls within the range of 15 to 66, accounting for 98.6%, with a mode of 40.5. The Ts_b distribution, on the other hand, shows a multimodal pattern, suggesting considerable variation in resilience across different regions. The highest proportion of samples is in the range of 5 to 10, accounting for 42.1%, with a mode of 7.5. This indicates that approximately 42.1% of the grid areas along the expressway take about 7 years to restore *Ts* to predisturbance levels. For ET_a, the frequency distribution also shows a right-skewed pattern, with the largest proportion of samples falling within the range of 0 to 0.6, accounting for 79.5%, with a mode of 0.3. The distribution for ET_b is similarly right-skewed, with the highest proportion of samples in the range of 0 to 5 and a mode of 2.5. This suggests that *ET* along the expressway typically recovers to predisturbance levels within about 2.5 years.

Optimal FGR configuration based on resilience characteristics

As shown in Fig. 6, a significant relationship exists between FGR and Res_{veg_clim} across different sections of the Hangrui Expressway. The black dots in the figure represent FGR values corresponding to different Res_{veg_clim} values. Analysis reveals a logarithmic relationship between these data points. A logarithmic function was fitted, and based on the characteristic of the resilience index, where smaller values correspond to stronger resilience, the inflection point of the fitted function was extracted. This point represents the optimal FGR, which marks the point at which vegetation resilience is maximized.

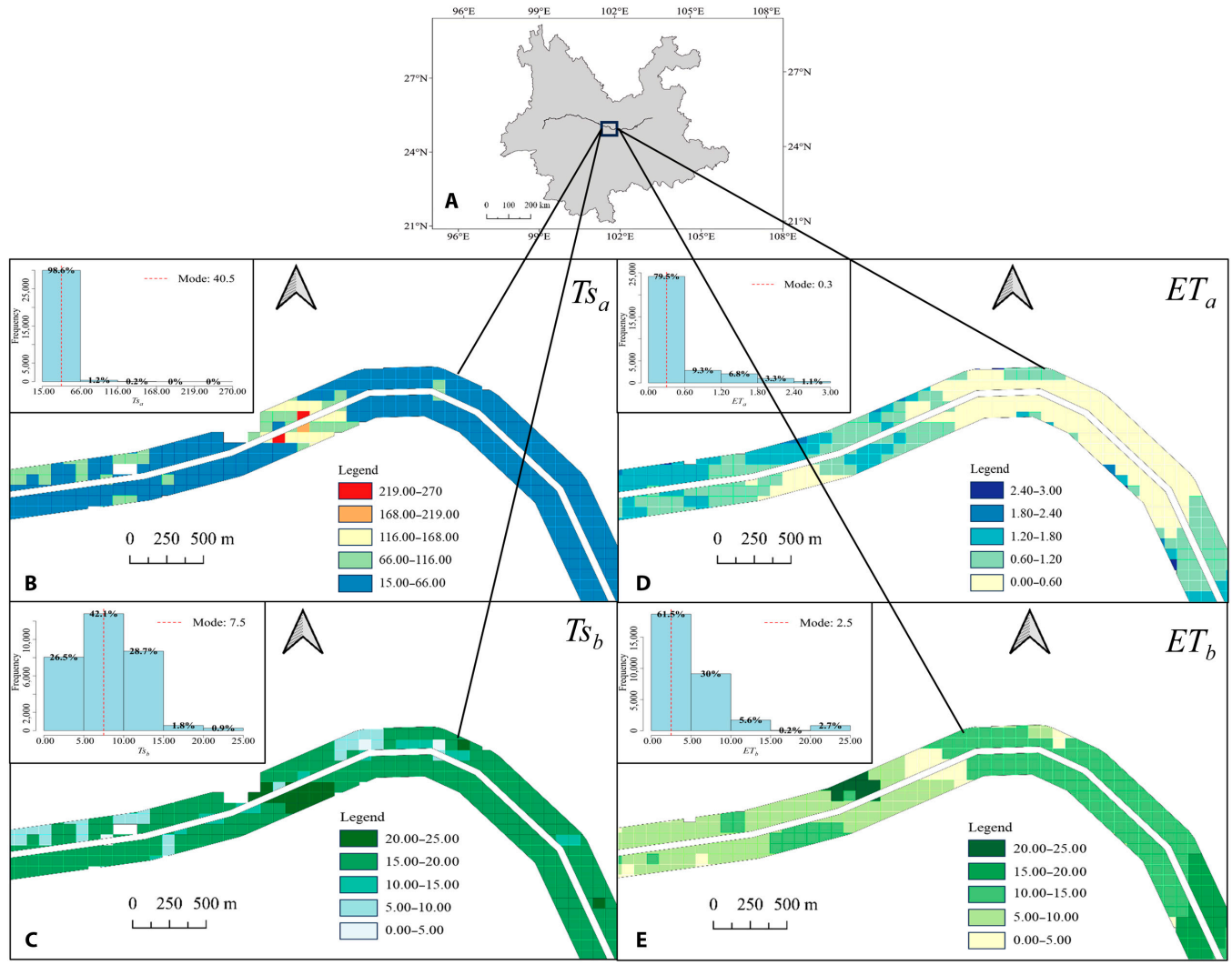

Fig. 5. The spatial distribution maps are based on locally enlarged sections of the Hangrui Expressway in Yunnan, while the frequency distribution charts are derived from data collected along the entire expressway. (A) Locations of the enlarged study sections within Yunnan Province. (B) Ts_a represents *Ts* resistance (range, 15 to 270), with darker colors indicating lower Ts_a values. (C) Ts_b represents *Ts* resilience (range, 0 to 25), with darker colors indicating lower Ts_b values. (D) ET_a represents *ET* resistance (range, 0 to 3.00), with darker colors indicating lower ET_a values. (E) ET_b represents *ET* resilience (range, 0 to 25), with darker colors indicating lower ET_b values.

The results indicate that the optimal FGR for the Kunming Second Ring Road section is 1:5, meaning that the area of trees and shrubs is one-fifth that of herbaceous vegetation. Within this FGR range, the artificial vegetation restoration effect on the expressway is most significant. The optimal FGR for the Kunming–Songming and Anning–Chuxiong sections are 3:10. For the Chuxiong–Dali, Dali–Baoshan, and Qujing–Songming sections, the optimal FGR is 1:2, indicating that vegetation resilience is greatest when the coverage of trees and shrubs is higher in these sections. The variation in the optimal FGR ratios across different segments reflects the unique vegetation configuration requirements of each section of the Hangrui Expressway in Yunnan.

Analysis of factors influencing resistance and resilience

The regression analysis results of environmental factors (slope, elevation, temperature, and precipitation) on different ecological function indicators (vegetation resistance and resilience, *Ts* resistance and resilience, and *ET* resistance and resilience) across different sections of the Hangrui Expressway in Yunnan are shown in the Fig. 7. The results indicate that the annual mean temperature generally has a significant impact on ecological functions. Annual mean temperature often enhances the stability of vegetation *ET* functions (e.g., in the Kunming Second Ring Road section and the Kunming–Songming section), but in some sections (e.g., the Anning–Chu section and the Dali–Baoshan section), it can inhibit the stability of vegetation and *Ts* functions. Annual mean precipitation is a key factor in most sections. Typically, precipitation inhibits ecosystem stability, especially vegetation and microclimate functions (e.g., the Kunming Second Ring Road section, the Chuxiong–Dali section, and the Dali–Baoshan section). The impact of elevation on microclimate stability and *ET* functions is more complex. In most cases, elevation has an inhibitory effect on microclimate stability but promotes evapotranspiration functions (e.g., in the Chuxiong–Dali section and the Dali–Baoshan section).

The structural equation model analysis results indicate that temperature, elevation, slope, and FGR have a significant positive impact on the Ts_b index ($ResIndex_{Ts}$), with path coefficients of 0.52,

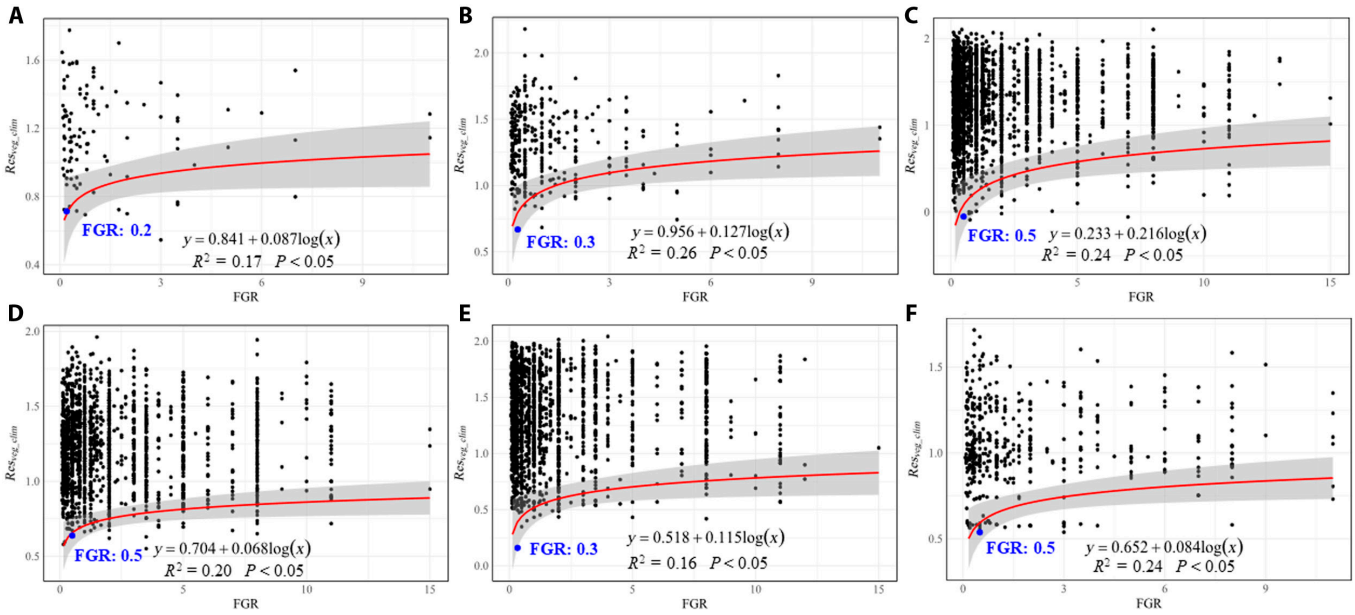

Fig. 6. Logarithmic function fitting results of the optimized forest–grassland ratio (FGR) and Res_{veg_clim} (combined performance of vegetation structure and function) across different segments of the Hangrui Expressway in Yunnan: Kunming Second Ring Road (A), Kunming–Songming segment (B), Chuxiong–Dali segment (C), Dali–Baoshan segment (D), Anning–Chuxiong segment (E), and Qujing–Songming segment (F). The black dots represent FGR values corresponding to different Res_{veg_clim} values, the red curve is the logarithmic function, the gray-shaded area represents the confidence interval, and the blue dots represent the optimal FGR.

0.52, 0.18, and 0.04, respectively. Only the duration of vegetation recovery has a significant negative impact on the $ResIndex_{Ts}$, with a path coefficient of −0.03. Temperature, precipitation, elevation, FGR, and vegetation recovery duration have a significant positive impact on the microclimate resilience index (*ResIndex*) and ET_b index ($ResIndex_{ET}$), with path coefficients of 0.38, 0.23, 0.09, 0.01, and 0.07, respectively. Only slope has a significant negative impact on the $ResIndex_{ET}$, with a path coefficient of −0.05. Temperature, precipitation, and elevation have a significant negative impact on the vegetation resilience index ($ResIndex_{NDVI}$), with path coefficients of −0.13, −0.06, and −0.09, respectively, while slope has a significant positive impact, with a path coefficient of 0.09. Overall, temperature, precipitation, elevation, and slope have a noticeably negative impact on vegetation resilience. However, vegetation growth conditions and recovery time have a positive effect on improving vegetation resilience. In addition, vegetation recovery can also promote the recovery of *Ts* and *ET*. The SEM explained 6%, 7%, and 1% of the variance in $ResIndex_{Ts}$, $ResIndex_{ET}$, and $ResIndex_{NDVI}$, respectively ($R^2 = 0.06$ to 0.07). According to Cohen's criterion, these correspond to small-to-moderate overall effect sizes ($f^2 \approx 0.06$ to 0.08).

Temperature, precipitation, elevation, slope, FGR, and recovery years can directly influence the resilience of underlying surface microclimate factors. They can also indirectly impact these factors by altering vegetation resistance–resilience. By calculating the product of direct and indirect connection paths and summing them according to different driving factors, the factors with the greatest impact on the outcome variable are identified (Fig. 8); it is evident that the coupling relationship between topographic factors and the microclimate resilience index exhibits positive feedback, significantly regulating *Ts*. Climate factors have different effects on the 3 resilience indices. They show a positive feedback relationship with $ResIndex_{Ts}$ and $ResIndex_{ET}$ but a negative one with $ResIndex_{NDVI}$.

Discussion

Spatiotemporal heterogeneity on the resistance and resilience of vegetation and microclimate effects

Road construction and expansion impose multiscale and persistent disturbances on ecosystems. These activities fundamentally reduce the resistance and resilience of adjacent habitats by causing habitat loss for plants and animals and introducing various pollutants [33,34]. Although artificial vegetation restoration measures are often implemented after construction, restoring ecosystem resistance and resilience remains a major challenge. Understanding the spatial distribution patterns of these 2 capacities and their driving mechanisms is therefore essential for managing human-dominated landscapes effectively. After restoration, vegetation shows clear resistance–resilience trade-offs: Stands closer to expressways tend to exhibit stronger disturbance resistance, whereas those farther away display higher recovery resilience. This spatial dichotomy likely stems from interactive effects between direct ecological disturbances from road construction and restoration interventions [35]. Proximity to expressways benefits from intensive artificial restoration, enabling vegetation to maintain high resistance against external disturbances. Conversely, areas farther from roads retain higher intrinsic recovery potential; despite persistent disturbances, reduced disturbance intensity allows rapid reestablishment of predisturbance ecological states—a pattern consistent with the seminal work on road ecology by Forman and Alexander [36]. Collectively, vegetation restoration mediates the interplay between construction impacts and mitigation measures, playing a pivotal role in fortifying disturbance resistance and accelerating ecosystem recovery trajectories.

As a pivotal regulator of ecosystem structure and function, vegetation microclimate governs biogeochemical cycling and energy flux by modulating soil biota activity, vegetation

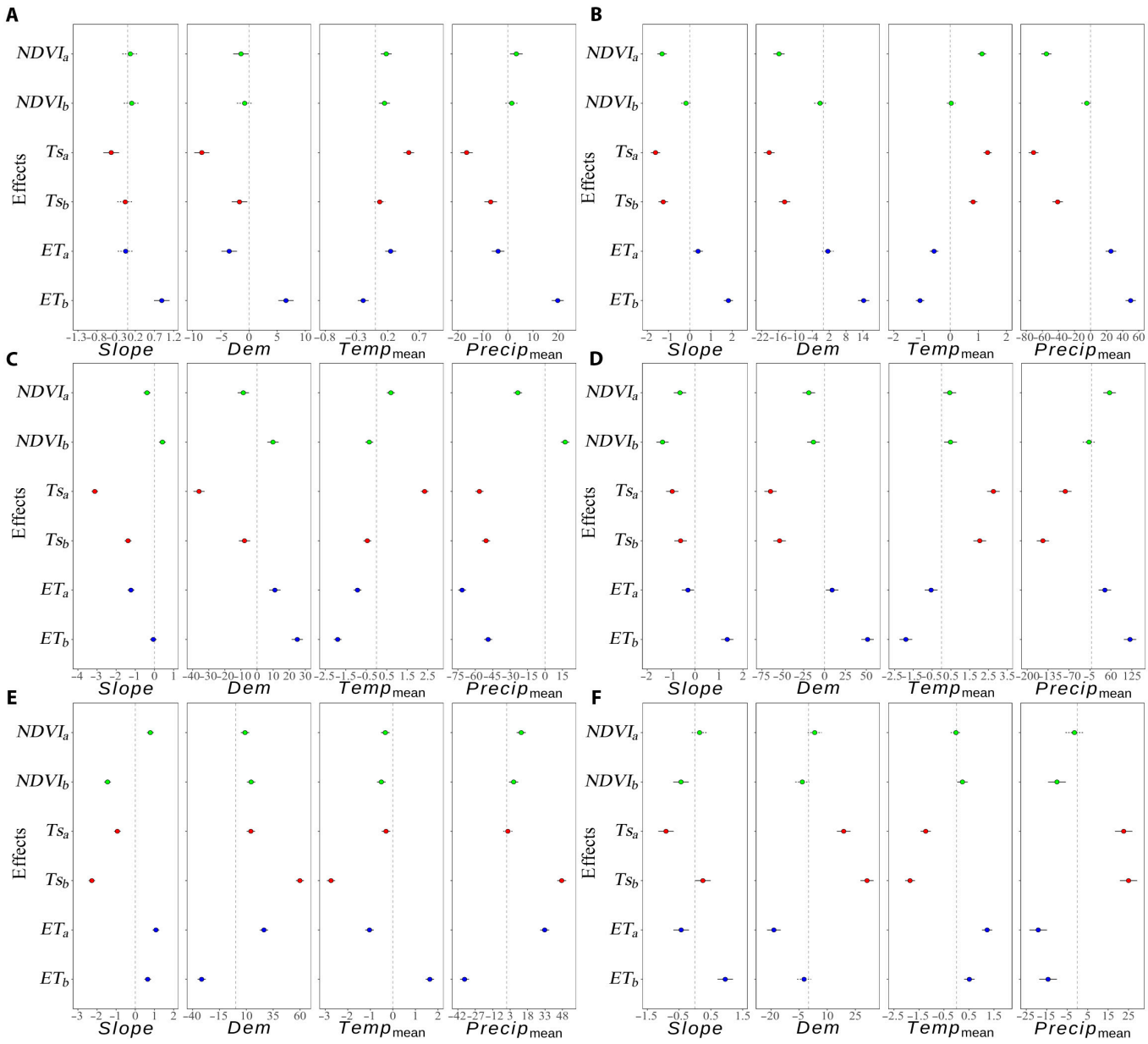

Fig. 7. Regression relationship between vegetation and microclimate resistance–resilience with environmental factors across different segments of the Hangrui Expressway in Yunnan is shown for each section as follows: Kunming Second Ring Road (A), Kunming–Songming segment (B), Chuxiong–Dali segment (C), Dali–Baoshan segment (D), Anning–Chuxiong segment (E), and Qujing–Songming segment (F).

growth-physiological processes, and species distribution patterns [37]. Road construction drastically reshapes local microclimatic regimes, intensifying road-adjacent urban heat island effects and disrupting hydrological cycles. These alterations constitute persistent ecological stressors that engage in complex feedback loops with vegetation recovery processes [34,38]. Analysis of microclimatic factors reveals spatiotemporal patterns in Ts_a and resilience mirroring vegetation dynamics: Areas distal to expressways exhibit accelerated temperature recovery to baseline levels, demonstrating restoration-enhanced thermal stability. While road development profoundly alters microclimate through localized heat island amplification, particularly along expressway corridors where pronounced thermal fluctuations challenge microclimatic recovery, artificial restoration interventions effectively mitigate such effects. Empirical evidence from temperature resilience metrics confirms that restoration measures substantially dampen thermal variability amplitude and shorten recovery duration, with optimal outcomes observed in well-restored zones. In terms of *ET*, areas near the expressway exhibit increased moisture stability and stronger ET_a due to increased vegetation cover. This indicates that surrounding vegetation, by increasing ground cover, regulates the local microclimate cycle, improves microclimate conditions, and enhances local moisture stability. These findings highlight the crucial role of artificial restoration measures in accelerating water balance recovery and enhancing the stability of the microclimate cycle. Future road construction and ecological restoration efforts should carefully consider these interactions to improve the efficiency and sustainability of ecological restoration.

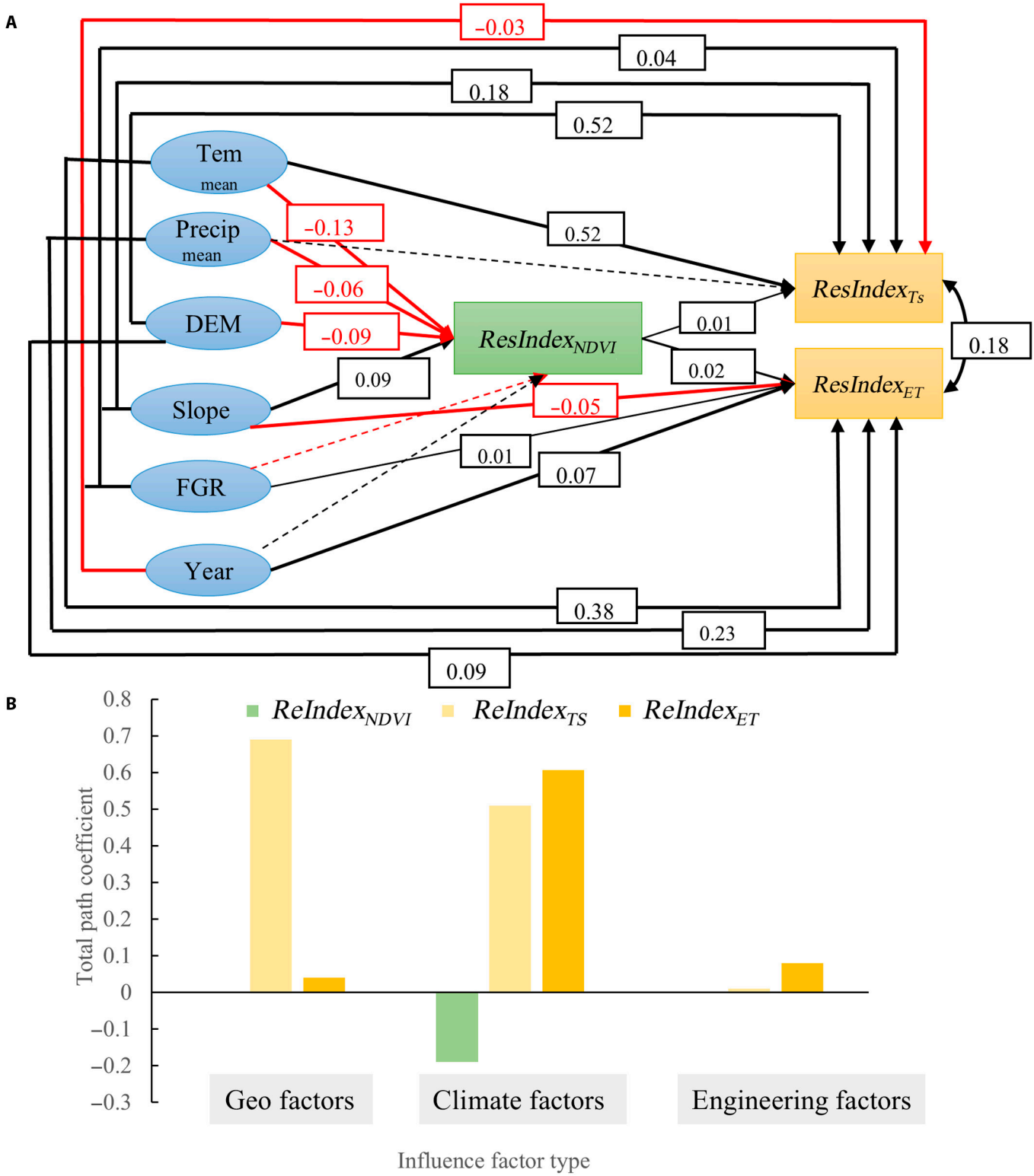

Fig. 8. (A) Structural equation model of vegetation and microclimate resilience indices along the Hangrui Expressway in Yunnan. (B) Quantitative results of the structural equation model for vegetation and microclimate resilience indices along the Hangrui Expressway in Yunnan. (Overall model fitness: Fisher's $C = 0$, Akaike information criterion = 52, $P = 1$).

The impact of regional FGR on ecological resilience

Vegetation structure substantially influences ecosystem stability and resilience. In general, trees lead the recovery process, providing long-term ecological services such as carbon sequestration and habitat provision [39]. Shrubs play a crucial role in buffering extreme climatic changes and providing ecological connectivity [35]. Herbaceous plants possess rapid growth capacity, enabling them to quickly cover bare soil during the early stages of disturbance, thereby reducing erosion and restoring soil fertility [39]. Structural diversity helps enhance ecosystem complexity and

stability, thereby aiding ecosystems in withstanding pressures such as climate change and land-use changes [40]. Consequently, ecosystems optimize resilience by adjusting the proportional distribution of trees, shrubs, and herbaceous plants within the community (e.g., FGR) to leverage the complementary advantages of these vegetation types. Our study found that adjusting vegetation structure based on the ecological conditions of road segments can significantly enhance restoration efficiency, which aligns with the ecological restoration theory proposed by Clewell and Aronson [41]. In the Dali–Baoshan and Chuxiong–Dali segments, favorable climatic conditions and mountainous and hilly landscapes result in an optimal FGR with a higher proportion of trees and shrubs, demonstrating strong ecological recovery potential. In contrast, in highly urbanized and urban agglomeration areas such as Kunming Second Ring Road, Kunming–Songming, and Anning–Chuxiong segments, where vegetation resilience is lower, the optimal FGR includes a higher proportion of herbaceous plants. As Zhao and Running [42] emphasized, herbaceous plants play a essential role in rapid *ET* regulation, regulating the microclimate cycle and facilitating the better adaptation of peri-urban ecosystems to rapidly changing environmental conditions. Optimizing FGR based on ecological conditions can significantly enhance ecosystem stability and resilience, providing a scientific basis for implementing restoration projects.

The impact of influence factors on ecological resilience

Spanning over 1,000 km across Yunnan Province, our investigation traverses diverse climatic regimes, topographies, and vegetation types, driving substantial variations in vegetation and microclimatic resistance or resilience along expressway corridors. Critically, geographic factors (particularly slope and DEM) exert statistically significant negative impacts on vegetation resilience and resistance across nearly all segments. Steep slopes compromise soil stability, accelerating topsoil nutrient loss [43], thereby disrupting plant establishment and impairing both resistance and resilience—while moderate slopes may facilitate limited water infiltration and nutrient accumulation in some semiarid regions [44]. Our study area contains a large number of steep slopes generated by road construction projects that have undergone ecological restoration; this specific background may further amplify the one-way negative impact of slopes, as restored slopes often retain fragmented soil structure and limited nutrient storage despite restoration efforts. DEM increase adversely affects vegetation not only through thermal-deficit-induced growth retardation but also via photoactive radiation enhancement that impairs photosynthetic systems, suppresses carbon assimilation, and reduces foliar longevity—collectively diminishing plant resilience and resistance, a pattern empirically corroborated by Freund et al. [45] and Liu et al. [46]. The drive of climate factors offers opportunities for Ts_a, Ts_b, ET_a, and ET_b. Ts_a and Ts_b along nearly all roads showed a significant positive correlation with the annual average temperature, while ET_a and ET_b were significantly negatively correlated with the same. This may be because rising annual temperatures promote vegetation growth and recovery, increase *ET*, and help *Ts* remain relatively stable despite the rising trend in annual temperatures [47]. By extrapolating the relationships identified in this study between vegetation structure, microclimate stability, and ecological resilience, the research offers a scalable model for mitigating the environmental impacts of road construction. In addition, the study emphasizes the critical role of artificial restoration measures in accelerating ecosystem recovery and enhancing vegetation stability, providing a new perspective for integrating infrastructure development with ecological restoration in the future [48,49].

In addition, in the SEM results, although several standardized pathway coefficients were numerically small (like <0.05), their ecological implications should not be underestimated. In complex terrestrial ecosystems, weak but directionally consistent effects often act in concert, resulting in cumulative or network-mediated responses that are ecologically meaningful even when individual pathways appear minor. The observed overall explained variance ($R^2 = 0.06$ to 0.07; $f^2 \approx 0.06$ to 0.08) falls within the range typically reported for large-scale environmental models, where multiple interacting factors jointly determine biophysical indices such as *Ts* and *ET*. From an ecological standpoint, such small standardized effects can still represent meaningful processes when they are spatially pervasive or persist through time. A 0.04 to 0.05 standardized change, when integrated across thousands of grid cells or consecutive years, may translate into observable shifts in energy and water fluxes. Therefore, we interpret the small pathway coefficients as indicators of diffuse but coherent environmental influences, rather than statistical noise.

Limitations of the study

This study has certain limitations. First, it primarily relies on remote sensing data with a spatial resolution of 30 m and a 200-m buffer zone around the focal road segments. The choice of a 200-m buffer was made after preliminary testing, balancing the actual spatial configuration of roadside vegetation, data availability, and the requirement for long-term time-series monitoring. At the landscape scale, this buffer range was found to be the most appropriate for capturing vegetation recovery processes, assessing environmental drivers, and evaluating microclimatic effects of ecological restoration. However, for finer-scale ecological or engineering analyses, such as species-level planting design, slope stabilization on roadside microtopography, or detailed stand structure characterization, a narrower buffer zone (e.g., 50 to 100 m) combined with higher-resolution remote sensing (e.g., unmanned aerial vehicle- or near-ground observations) would be more suitable. Such datasets can better resolve local gradients but are often limited by temporal coverage and continuity. Therefore, the optimal buffer size and spatial resolution should ultimately be determined by the specific research objectives and data availability.

Second, although the study reveals spatiotemporal correlations between vegetation and microclimate factors, it does not explore their causal mechanisms. Inferring causality requires long-term observational data and advanced dynamic system modeling. In addition, due to the limitations of remote sensing imagery on time scales, the exact number of years needed for vegetation restoration in different climate zones cannot be accurately assessed. Future research should integrate ground-based meteorological data with remote sensing to comprehensively analyze vegetation and microclimate dynamics, potentially uncovering the driving mechanisms behind these changes.

Conclusion

Based on multidecadal remote sensing monitoring of a major east–west expressway in Yunnan, China, this study evaluated

the dynamics and stability of the roadside ecosystem. The key indicators regarding the resistance and resilience of the vegetation and microclimate were developed to quantify the optimal FGR across different areas. The results reveal that the spatial heterogeneity of ecosystem resilience along the subtropical expressway is driven by a hierarchical regulatory mechanism. Regionally, climate acts as the primary determinant governing the baseline trajectory of vegetation recovery. Locally, however, the stability of the microclimate environment is distinctly modulated: geographical factors dominate thermal regulation (*Ts*), while the restoration engineering measures control the moisture regime (*ET*). Besides these interactions, it had been identified that a specific canopy structure, an optimal FGR of 0.3 ± 0.13 on average maximizes the system's restoration stability. The results showed that vegetation recovery generally required about 4 years, whereas *Ts* and *ET* took approximately 7 and 2 years, respectively, to return to predisturbance levels. This study provides a novel quantitative approach for assessing the structural and functional stability of ecosystems, which can be widely applied under similar environmental conditions to evaluate restoration effectiveness and optimize the design and implementation of artificial interventions.

Acknowledgments

Funding: This work was supported by the National Key Research and Development Program of China (grant numbers 2023YFF1304305 and 2021YFB2600104), the National Natural Science Foundation of China (grant number 32101324), High-Level Foreign Experts Introducing Program (G2023109009L), and Open Fund Project of the Key Laboratory of Surface Process Analysis and Modeling, Ministry of Education, Peking University.

Author contributions: J.G. and W.G. contributed to the research design, data analysis, and manuscript writing. B.D.F. and Z.L. contributed through conceptualization, formal analysis, supervision, and writing—review and editing. F.P. was responsible for visualization and data curation. H.S. contributed to visualization and manuscript writing. J.C. was responsible for visualization and project administration. Y.K. was responsible for data collection. S.T. revised the manuscript. G.S. acquired funding and supervised the project. All authors discussed the results and approved the final version of the manuscript.

Competing interests: The authors declare that they have no competing interests.

Data Availability

The datasets generated during and/or analyzed during the current study are available from the corresponding author on reasonable request.

References

1. Holling CS. Resilience and stability of ecological systems. *Annu Rev Ecol Syst*. 1973;4(1):1–23.
2. Gauch HG Jr, Whittaker RH, Wentworth TR. A comparative study of reciprocal averaging and other ordination techniques. *J Ecol*. 1977;65(1):157–174.
3. Pimm SL. The complexity and stability of ecosystems. *Nature*. 1984;307:321–326.
4. Intergovernmental Panel on Climate Change (IPCC). *Climate change 2022 – Impacts, adaptation and vulnerability: Working group II contribution to the sixth assessment report of the Intergovernmental Panel on Climate Change*. Cambridge (UK): Cambridge University Press; 2023.
5. Qin JX, Hao XM, Hua D, Hao HC. Assessment of ecosystem resilience in Central Asia. *J Arid Environ*. 2021;195: Article 104625.
6. Karsai I, Schmickl T, Kampis G. *Resilience and stability of ecological and social* systems. Cham: Springer International Publishing; 2020.
7. Zhou YY, Fu DJ, Lu CX, Xu XM, Tang QH. Positive effects of ecological restoration policies on the vegetation dynamics in a typical ecologically vulnerable area of China. *Ecol Eng*. 2021;159:Article 106087.
8. Holling CS. Understanding the complexity of economic, ecological, and social systems. *Ecosystems*. 2001;4(5):390–405.
9. Cushman SA, McGarigal K. Metrics and models for quantifying ecological resilience at landscape scales. *Front Ecol Evol*. 2019;7:440.
10. Tong Y, Lei J, Zhang S, Zhang X, Rong T, Fan L, Duan Z. Analysis of the spatial and temporal variability and factors influencing the ecological resilience in the urban agglomeration on the northern slope of Tianshan mountain. *Sustainability*. 2023;15(6):4828.
11. Shi C, Zhu X, Wu H, Li Z. Assessment of urban ecological resilience and its influencing factors: A case study of the Beijing-Tianjin-Hebei urban agglomeration of China. *Land*. 2022;11(6):921.
12. Jia X, Zhou W, Lei T, Jing L, Shen Y. Impact analysis of expressway construction on ecological carrying capacity in the Three-River Headwater region. *J Traffic Transp Eng Engl*. 2020;7:700–714.
13. Li C, Zhang J, Philbin SP, Yang X, Dong Z, Hong J, Ballesteros-Pérez P. Evaluating the impact of highway construction projects on landscape ecological risks in high altitude plateaus. *Sci Rep*. 2022;12(1):5170.
14. Li Q, Shi X, Wu Q. Exploring suitable topographical factor conditions for vegetation growth in Wanhuigou catchment on the Loess Plateau, China: A new perspective for ecological protection and restoration. *Ecol Eng*. 2020;158: Article 106053.
15. Zhang J, Hu R, Cheng X, Christos V, Philbin SP, Zhao R, Zhao X. Assessing the landscape ecological risk of road construction: The case of the Phnom Penh-Sihanoukville Expressway in Cambodia. *Ecol Indic*. 2023;154:Article 110582.
16. Wang Y, Li Z, Zheng X. The microclimatic effects of ecological restoration in brownfield based on remote sensing monitoring: The case studies of landfills in China. *Ecol Eng*. 2020;157:Article 105997.
17. Hou X, Liu S, Zhao S, Zhang Y, Wu X, Cheng F, Dong S. Interaction mechanism between floristic quality and environmental factors during ecological restoration in a mine area based on structural equation modeling. *Ecol Eng*. 2018;124:23–30.
18. Li Z-Y, Ye X-Z, Wang S-P. Ecosystem stability and its relationship with biodiversity. *Chin J Plant Ecol*. 2021;45(10):1127–1139.
19. Che M, Yang F, Sun J, Zhang C, Zhang J. Influence of road network expansion on the landscape ecological risk in the Yangtze River Delta region over the past two decades. *Ecol Indic*. 2023;156:Article 111178.

20. De Bello F, Lavorel S, Hallett LM, Valencia E, Garnier E, Roscher C, Conti L, Galland T, Goberna M, Májeková M, et al. Functional trait effects on ecosystem stability: Assembling the jigsaw puzzle. *Trends Ecol Evol*. 2021;36(9):822–836.
21. Tian H, Cao C, Chen W, Bao S, Yang B, Myneni RB. Response of vegetation activity dynamic to climatic change and ecological restoration programs in Inner Mongolia from 2000 to 2012. *Ecol Eng*. 2015;82:276–289.
22. Zeng L, Wardlow BD, Xiang D, Hu S, Li D. A review of vegetation phenological metrics extraction using time-series, multispectral satellite data. *Remote Sens Environ*. 2020;237:Article 111511.
23. Gu F, Xu G, Wang B, Jia L, Xu M. Vegetation cover change and restoration potential in the Ziwuling Forest region, China. *Ecol Eng*. 2023;187:Article 106877.
24. Sun H, Wang C, Niu Z. Analysis of the vegetation cover change and the relationship between NDVI and environmental factors by using NOAA time series data. *J Remote Sens*. 1998;2:210–216.
25. Teuling AJ, Seneviratne SI, Stöckli R, Reichstein M, Moors E, Ciais P, Luyssaert S, van den Hurk B, Ammann C, Bernhofer C, et al. Contrasting response of European forest and grassland energy exchange to heatwaves. *Nat Geosci*. 2010;3:722–727.
26. Mauser W, Schädlich S. Modelling the spatial distribution of evapotranspiration on different scales using remote sensing data. *J Hydrol*. 1998;212–213:250–267.
27. Shao R, Wang Y, Shao W, Ni G. Assessing the synergistic modulation of evapotranspiration by global impervious surface and vegetation changes. *Agric For Meteorol*. 2022;327:Article 109194.
28. Yang J, Huang X. The 30 m annual land cover dataset and its dynamics in China from 1990 to 2019. *Earth Syst Sci Data*. 2021;13(8):3907–3925.
29. Li Z, Wang Z, Liu X, Fath BD, Liu X, Xu Y, Hutjes R, Kroeze C. Causal relationship in the interaction between land cover change and underlying surface climate in the grassland ecosystems in China. *Sci Total Environ*. 2019;647:1080–1087.
30. Li Z, Wu W, Liu X, Fath BD, Sun H, Liu X, Xiao X, Cao J. Land use/cover change and regional climate change in an arid grassland ecosystem of Inner Mongolia, China. *Ecol Model*. 2017;353:86–94.
31. Richter R, Schläpfer D. *Atmospheric/topographic correction for satellite imagery (ATCOR-2/3 User Guide, Version 9.0.0)*. Wessling (Germany): ReSe Applications Schläpfer; 2015.
32. Lefcheck JS. Piecewise SEM: Piecewise structural equation modelling in R for ecology, evolution, and systematics. *Methods Ecol Evol*. 2016;7:573–579.
33. Li G, Li Y, Ma F, Zhang J, Wang M, Zhao W, Huang Y, Meng X, Yue D. Evaluating the suitability of ecological restoration techniques in distinct ecoregions along the China-Nepal Highway. *Ecol Indic*. 2024;168:Article 112743.
34. Trombulak SC, Frissell CA. Review of ecological effects of roads on terrestrial and aquatic communities. *Conserv Biol*. 2000;14:18–30.
35. Hobbs RJ, Harris JA. Restoration ecology: Repairing the Earth's ecosystems in the new millennium. *Restor Ecol*. 2001;9(2): 239–246.
36. Forman RTT, Alexander LE. Roads and their major ecological effects. *Annu Rev Ecol Syst*. 1998;29:207–231.
37. Terschanski J, Nunes MH, Aalto I, Pellikka P, Wekesa C, Maeda EE. The role of vegetation structural diversity in regulating the microclimate of human-modified tropical ecosystems. *J Environ Manag*. 2024;360:Article 121128.
38. Gucinski H. *Forest roads: A synthesis of scientific information*. Portland (OR): US Department of Agriculture, Forest Service, Pacific Northwest Research Station; 2001.
39. Bond WJ. What limits trees in C_4 grasslands and savannas? *Annu Rev Ecol Evol Syst*. 2008;39:641–659.
40. Chapin FS III, Zavaleta ES, Eviner VT, Naylor RL, Vitousek PM, Reynolds HL, Hooper DU, Lavorel S, Sala OE, Hobbie SE, et al. Consequences of changing biodiversity. *Nature*. 2000;405:234–242.
41. Clewell AF, Aronson J. Motivations for the restoration of ecosystems. *Conserv Biol*. 2006;20:420–428.
42. Zhao M, Running SW. Response to comments on "drought-induced reduction in global terrestrial net primary production from 2000 through 2009". *Science*. 2011;333(6046):1093.
43. He J, Shi X, Fu Y. Identifying vegetation restoration effectiveness and driving factors on different micro-topographic types of hilly Loess Plateau: From the perspective of ecological resilience. *J Environ Manag*. 2021;289: Article 112562.
44. Bordoloi S, Ng CWW. The effects of vegetation traits and their stability functions in bio-engineered slopes: A perspective review. *Eng Geol*. 2020;275:Article 105742.
45. Freund CA, Clark KE, Curran JF, Asner GP, Silman MR. Landslide age, elevation and residual vegetation determine tropical montane forest canopy recovery and biomass accumulation after landslide disturbances in the Peruvian Andes. *J Ecol*. 2021;109(10):3555–3571.
46. Liu Y, Xiao P, Zhang X, Liu H, Chen S, Jia Y. Accelerated decline in vegetation resilience on the Tibetan Plateau. *Land Degrad Dev*. 2025;36(1):295–306.
47. Bradford JB, Schlaepfer DR, Lauenroth WK, Palmquist KA, Chambers JC, Maestas JD, Campbell SB. Climate-driven shifts in soil temperature and moisture regimes suggest opportunities to enhance assessments of dryland resilience and resistance. *Front Ecol Evol*. 2019;7:358.
48. Sánchez-Reyes UJ, Nio-Maldonado S, Barrientos-Lozano L, Carreón JT, Jones RW. Structural changes of vegetation and its association with microclimate in a successional gradient of low thorn forest in northeastern Mexico. *Plant Ecol*. 2021;222: 65–80.
49. Stickley SF, Fraterrigo JM. Understory vegetation contributes to microclimatic buffering of near-surface temperatures in temperate deciduous forests. *Landsc Ecol*. 2021;36:1197–1213.

Ecosystem Health and Sustainability
A SCIENCE PARTNER JOURNAL

Resistance and Resilience of Vegetation and Microclimate along the Subtropical Expressway via Remote Sensing

Jiali Gu, Wan Geng, Zhouyuan Li, Brian D. Fath, Fei Pan, Haiyue Shi, Jiding Chen, Yaping Kong, Shuangcheng Tao, and Guilong Song

Citation: Gu J, Geng W, Li Z, Fath B, Pan F, Shi H, Chen J, Kong Y, Tao S, Song G. Resistance and Resilience of Vegetation and Microclimate along the Subtropical Expressway via Remote Sensing. *Ecosyst Health Sustain*. 2026;**12**:0509.
DOI: 10.34133/ehs.0509

Evaluating vegetation resistance and resilience is key to understanding ecosystem responses to human disturbances such as road construction and to guiding ecological restoration. This study systematically assessed the resistance and resilience of vegetation and microclimate along the Hangrui Expressway in southwestern China using remote sensing techniques. Landsat imagery from 10 representative years between the preconstruction period (1993) and the recovery period (2021) was analyzed, with indicators such as the normalized difference vegetation index, surface temperature, and evapotranspiration used to characterize vegetation and microclimate. The study area was divided into 200-m buffer zones, and resistance–resilience indicators were developed to reveal spatial distribution patterns. In addition, an optimized "forest–grassland ratio" was proposed to guide vegetation configuration strategies, effectively promoting the enhancement of both vegetation and microclimate resilience. Structural equation modeling identified the key factors influencing roadside vegetation resistance and resilience. The results showed that most areas exhibited strong resistance and resilience, enabling rapid recovery after disturbances. Vegetation typically required about 4 years to recover, while surface temperature and evapotranspiration required 7 and 2 years, respectively, to return to predisturbance levels. Topographic factors were significantly positively correlated with microclimate resilience, while climate factors were positively correlated with microclimate resilience but negatively correlated with vegetation resilience. Climate and topography were the main influencing factors. The optimal forest–grassland ratio varied across different regions. These findings underscore the importance of considering local climatic and topographic conditions in road planning and ecological restoration to improve restoration outcomes and promote ecosystem stability.
Image